

# Control Relevant Identification and Robust Motion Control of a Wafer Stage

Raymond A. de Callafon<sup>1</sup> and Paul M.J. Van den Hof<sup>2</sup>

<sup>1</sup> Department of Mechanical and Aerospace Engineering, University of California at San Diego, 9500 Gilman Drive, La Jolla, CA 92093-0411, USA

<sup>2</sup> Signals, Systems and Control Group, Department of Applied Physics, Delft University of Technology, 2628 CJ Delft, The Netherlands

**Abstract.** This chapter illustrates the identification of control-relevant models and the subsequent robust control design applied to a wafer stage. A wafer stage is part of a wafer stepper and used in chip manufacturing processes for accurate positioning of the silicon wafer on which the chips are to be produced. Accurate and fast positioning requires a robust and high-performance multivariable servo controller that enables a fast throughput of silicon wafers. An advanced servo controller is developed by an iterative procedure of control-relevant model identification including model uncertainty bounding, and robust control based on worst-case performance optimization. Both stability and performance robustness can be monitored, enabling the possibility to guarantee performance improvement in a single step of the iteration. This is shown to lead to a successful design and implementation on a wafer stage set-up.

## 1 Introduction

The overlapping theme in the application discussed in this chapter, is the robust and enhanced control of a mechanical positioning mechanism. The methodology presented and illustrated in this chapter is applicable to many mechanical systems that are subjected to high-performance servo positioning demands. The dedicated servo positioning mechanism considered in this chapter can be found in a wafer stepper. Wafer steppers combine a high-accuracy positioning and a sophisticated lithographic process to manufacture integrated circuits (chips) via a fully automated process.

By means of a photolithographic process, the chip architecture is exposed on the surface of a wafer, a silicon disk covered with photo resist. Typically, the wafer can carry more than 80 chips and in order to expose the surface of the wafer, each chip has to be processed sequentially. Such a sequential process is needed as only one mask of the chip layout is available during the exposure phase of the photolithographic process. In order to enable sequential processing, the wafer is mounted on a wafer stage that needs to be accurately moved (stepped) in 3 Degrees Of Freedom (3DOF).

Both the accuracy and the speed of the wafer stage will influence the success and throughput of the production process of the chips on the wafer. Sophisticated design and control of this multivariable servo mechanism can

help in achieving a required throughput. An important design step is the construction of a servo controller that is able to satisfy high-performance requirements: fast positioning to within an accuracy of  $\pm 52nm$ . The inherent multivariable (3DOF) nature of the wafer stage and the high positioning performance requirements require a servo design approach in which the dynamic behavior of the positioning mechanism is characterized accurately.

The required accuracy of the dynamical model will be dictated by the performance requirements imposed on the control system; additionally low complexity (approximate) models are desired in order to limit the complexity of the subsequent control design and implementation. As a result the modeling procedure will be subjected to the following basic requirements.

- A (nominal) model should be of low complexity and approximate the dominant dynamical behavior that is relevant for high-performance control design;
- to address stability and performance robustness and facilitate the design of a robust performing controller, a nominal model should be accompanied with a bound on its uncertainty;
- closely related to the development of a nominal model, the size and shape of this model uncertainty is implicitly bounded by the requirements for high-performance control design.

Inevitably, low complexity (nominal) models and a small model uncertainty are conflicting requirements. For high-performance servo control requirements, the trade-off between approximation and uncertainty provides a challenging modeling procedure. In the application of the wafer stage mechanism discussed in this chapter, the above mentioned requirements are tackled by adopting an identification framework in which a control relevant set of models is formulated and estimated on the basis of closed-loop experiments. Subsequently this set is used as a basis for a robust control design, finding the best worst-case controller.

## 2 The Wafer Stepper Positioning Mechanism

### 2.1 Description of servo mechanism

The wafer stage servo mechanism is an integral part of a Silicon Repeater 3rd generation (SIRE3) wafer stepper. The wafer stage is used to accurately position the silicon wafer on which the chips are to be produced. A schematic picture of the stage is shown in Figure 1.

The wafer chuck is part of the wafer stage and is equipped with an air bearing and placed on a large suspended granite block to reduce the effect of external vibrations. The wafer chuck is used to position the wafer in 3 Degrees Of Freedom (3DOF) along the surface of the granite block. As part of the mechanical positioning mechanism, three linear voice coil motors are

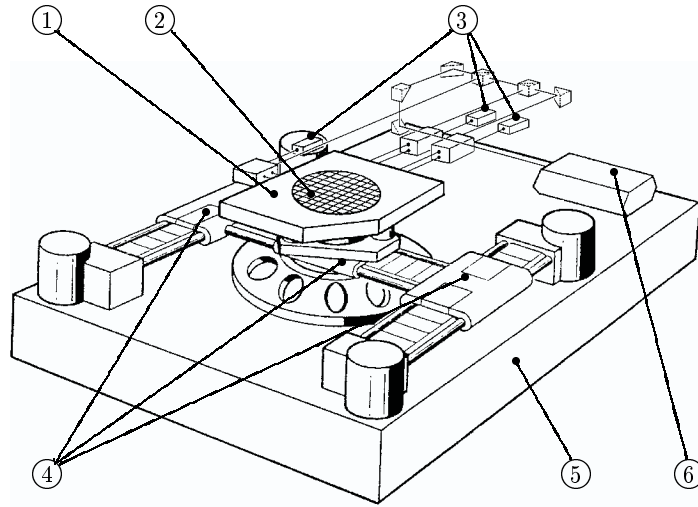


**Fig. 1.** Schematic view of a wafer stage; 1: mirror block, 2: wafer chuck, 3: laser interferometers, 4: linear motors, 5: granite block, 6: laser.

mounted in a H-shape on the granite block. The three linear motors are used to position the wafer chuck in 3DOF along the surface of the granite block. Independent steering of the motors enables free surface translation with a relatively small rotational freedom.

The position in the horizontal plane is measured by means of laser interferometry. Relative movements are measured by determining the phase shift of the laser beams reflected on the mirror block depicted in Figure 2. As the horizontal plane allows three degrees of freedom, three laser measurements uniquely determine the horizontal position of the wafer.

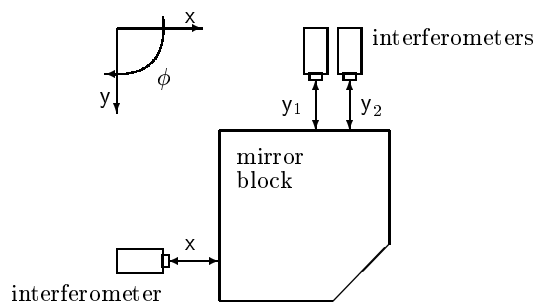


**Fig. 2.** The three position measurements on the mirror block

The three position measurements can be used to reconstruct the position of the stage in  $x$ -,  $y$ - and  $\phi$ -direction. From the three (relative) position measurements given in Figure 2, the three degrees of freedom of the stage in  $x$ -,  $y$ - en  $\phi$ - direction can be obtained via

$$\begin{bmatrix} x \\ y \\ \phi \end{bmatrix} = T \begin{bmatrix} x \\ y_1 \\ y_2 \end{bmatrix} \quad \text{with } T := \begin{bmatrix} 1 & 0 & 0 \\ 0 & 1/2 & 1/2 \\ 0 & 1/2 & -1/2 \end{bmatrix}.$$

The transformation matrix  $T$  statically decouples the two measurements  $y_1$  and  $y_2$  in the  $y$ -direction. However note that  $\phi = (y_1 - y_2)/2$  is not the actual rotation of the stage, as this would require the computation involving a sinusoidal term. However, the rotation of the stage is limited and for small difference between  $y_1$  and  $y_2$ , *e.g.*, small rotations, the value of  $\phi$  is proportional to the angular rotation of the stage.

The three independent linear motors and the laser positioning measurements make the servo mechanism of the wafer stepper a multivariable system. The inputs reflect the currents to the three linear motors, whereas the outputs are the positions of the wafer chuck both in  $x$ -,  $y$ -direction (translation) and in  $\phi$ -direction (rotation).

## 2.2 Experimental set up

In order to gather experimental data for system identification purposes and to test the servo control of the wafer stage, an experimental set up has been provided by Philips Research Laboratories. A close up photograph of the set up is provided in Figure 3; it the granite block and the wafer stage protected by a glass surface on top.

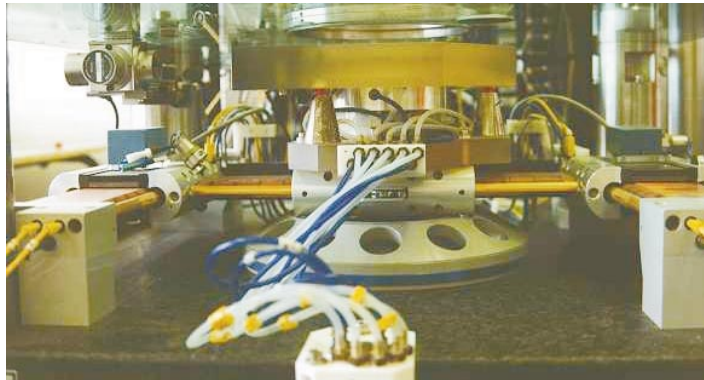


**Fig. 3.** Close-up of wafer stage displaying the three linear motors and the wafer chuck with air bearing

The experimental setup is equipped with a computer interface to measure the position in  $x$ -,  $y$ - and  $\phi$ -direction of the wafer chuck on discrete time samples via a digital signal processor. Due to safety requirements and operating conditions of the laser interferometers, the signals can be measured only if a digital controller is used to control the positioning of the wafer chuck. Such a digital controller can be implemented using the same digital signal processor. A schematic overview of the signals that can be accessed is depicted in the block diagram of Figure 4.

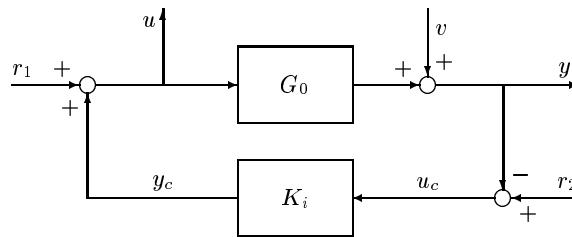


**Fig. 4.** Block diagram of experimental set up of feedback controlled positioning mechanism

As indicated in Figure 4, the positioning mechanism of the wafer chuck is denoted by  $G_0$ , while the (initial) feedback controller currently used to control  $G_0$  is denoted by  $K_i$ . For notation purposes, the feedback connection of  $G_0$  and  $K_i$  is denoted by  $\mathcal{T}(G_0, K_i)$ .

The input  $u$  is used to indicate the three input signals to the linear motors for position actuation in  $x$ -,  $y$ - and  $\phi$ -direction. In a similar way, the output signal  $y$  consists of the three position signals in  $x$ -,  $y$ - and  $\phi$ -direction of the wafer chuck. Besides providing sufficient excitation of the feedback system, the reference signals in Figure 4 can be used to move or step the wafer chuck in a desired direction. As such, the signals  $r_1$  and  $r_2$  can be used to evaluate the performance of the feedback controlled plant by applying a reference signal  $r_2$  and a feed forward signal  $r_1$  in order to track a certain desired 3DOF position signal  $y$  of the wafer chuck. The input signal  $u_c$  to the controller  $K_i$  reflects the servo error between a desired reference  $r_2$  and the actual desired position  $y$ .

### 2.3 Modeling and servo performance of the positioning mechanism

In the conventional closed-loop servo control, the servo controller  $K_i$  consists of 3 parallel PID controllers. In this situation the interaction in the 3DOF positioning mechanism is clearly neglected, and the PID controllers are able to achieve only moderate control performance.

Servo performance requirements desire a minimization of the servo error, while moving the chuck as fast as possible. The design specification for the SIRE3 wafer stepper is to bring the servo error within a bound of 52nm (4 times the measurement resolution) as soon as possible after a step trajectory has been performed. This is due to the fact that the chuck must be kept in a constant position before a chip can be exposed on the surface of the wafer.

In order to compare the servo performance of (newly designed) feedback controllers, the reference signals  $r_2$  and  $r_1$  are fixed to some prespecified desired trajectory for servo performance evaluation. This prespecified trajectory is based on the dominating open loop dynamical behaviour of the wafer stage  $G_0$  that is given by a double integrator, relating the force generated by the linear motors to the position of the wafer chuck. Based on this relatively simple model,  $r_2$  will denote a desired position profile, allowing a maximum speed and a maximum jerk (derivative of acceleration), whereas  $r_1$  denotes (a scaled) acceleration profile obtained by computing the second derivative of  $r_2$ . A typical shape of the reference signal  $r_2$  and the feed forward signal  $r_1$  to position the wafer chuck in either the x- or y- direction over 1cm is depicted in Figure 5.

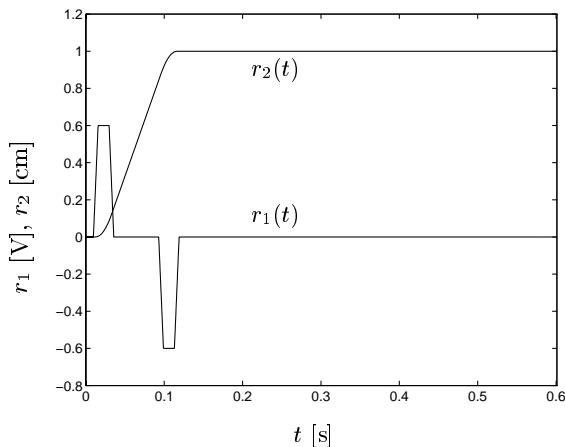


**Fig. 5.** Shape of reference signal  $r_2$  and feedforward signal  $r_1$  for servo performance evaluations

Although optimal reference signals can be designed for finite time optimal control problems, it should be noted that step wise reference signals are being used here *only* to compare the performance of the servo controllers being designed and actually implemented on the wafer stage.

The specified reference signals  $r_1$  and  $r_2$  in Figure 5 can be used to create a step in the  $x$ -direction for the evaluation of the performance of the 3 parallel

PID servo controllers. The resulting servo error  $u_{c,x}$  for a step in the  $x$ -direction is depicted in Figure 6.

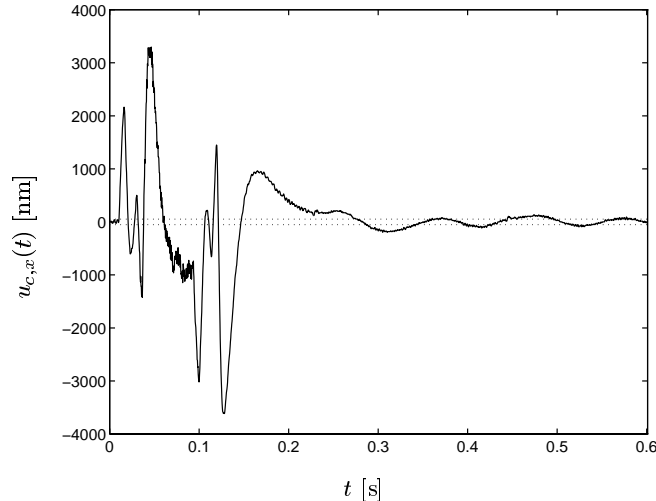


**Fig. 6.** Servo error response to a step in  $x$ -direction using conventional parallel PID controllers

It can be observed from Figure 6 that the servo error  $u_{c,x}$  is hardly within the bounds of 52nm indicated by the dotted lines, even after 0.6 s. Furthermore,  $u_{c,x}$  exhibits a low frequent vibration after the step has ended (after 0.12 s). As a result, the settling time of the positioning step is strongly influenced and both an improvement of the speed of decay and a reduction of the low frequent vibration of the servo error is desired to improve the behaviour of the servo mechanism. Clearly, the process under consideration exhibits dynamic phenomena additional to the simple model of a double integrator. Characterization of these dynamics in a way relevant for control design is essential in achieving maximum control performance.

For both the design of the feedback controller  $K_i$  and appropriate reference signals, a dynamic model of the wafer stage is required. In this chapter the attention is focused on the construction and use of dynamical models for the design of a feedback controller  $K_i$ .

## 2.4 Experiment Design

Experimental data from the wafer stage are gathered from the feedback connection  $\mathcal{T}(G_0, K_i)$  depicted in Figure 4. As mentioned in Section 2.3, the reference signals  $r_1$  and  $r_2$  are used to specify respectively an acceleration reference and a position reference profile to evaluate the servo performance of a feedback controller. However, from an identification point of view, the

reference signals are used to excite the closed-loop system  $\mathcal{T}(G_0, K_i)$  to avoid problems associated with closed-loop identifiability.

Although the signals  $r_1$  and  $r_2$  can be used to conduct identification experiments, mostly low frequent information is contained in the signals depicted in Figure 5. To get enough information on the system in the frequency range of interest, different reference signals have to be used. Furthermore, the flexibility of the experimental set up and the speed of the mechanical system allow the use of excitation signals to obtain a frequency response estimate of the positioning mechanism in the frequency range from approximately 10 Hz till 1 kHz.

For identification purposes the reference signals are specified as periodic signals constructed via a sum of sinusoids

$$r(t) := \sum_{i=1}^l \sin(\omega_i t + \phi_i) \quad (1)$$

specified at a predefined frequency grid  $\Omega = \{\omega \mid \omega = \omega_i, i = 1, 2, \dots, n\}$ . The phase shifts  $\phi_i$  in the sequence  $\{\phi_i\}$ ,  $i = 1, 2, \dots, l$  of (1) are chosen independently from a uniform distribution over the interval  $(-\pi, \pi)$ . In this way, the six<sup>1</sup> reference signals will be uncorrelated and a random phased sequence of sinusoids is generated with favourable properties [15].

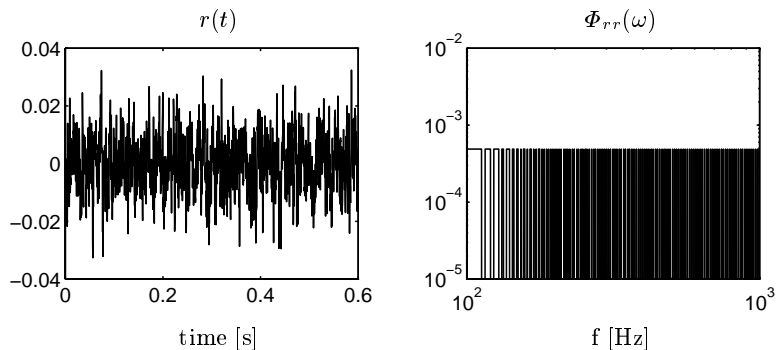


**Fig. 7.** Time domain plot (left) and spectrum (right) of the reference signal  $r_1$  in x-direction configured as a sum of 200 sinusoids with random phase

The designed excitation signals are periodic with a period length of 2048 data points sampled at  $T_s = 0.3ms$ . As a result, the frequency resolution  $\Delta f = 1/(2048 \cdot 0.003) \approx 1.628$  Hz. They are each composed of 200 sinusoids distributed (approximately logarithmically) between  $9 \times \Delta f \approx 14.65$  Hz and  $714 \times \Delta f \approx 1162.11$  Hz.

<sup>1</sup> Both  $r_1$  and  $r_2$  consist of three reference signals, respectively in x-, y- and  $\phi$ -direction.

For illustration purposes, a time domain plot and the spectrum density in the frequency range between 100 Hz and 1 kHz of one of the six reference signals is shown in Figure 7. It can be observed that the signal has a well bounded amplitude. Although the signal looks like a noise in the time domain, the spectrum is very well defined for the 200 frequency points in the frequency grid  $\Omega$ . With these reference signals the identification experiments have been performed. They will be further explained and analyzed in the sequel of this chapter.

### 3 Iterative Model Set Estimation and Control Design

#### 3.1 Motivation of model set estimation

The motivation to apply an iterative procedure of identification and control is induced by the fact that a simultaneous (off-line) optimization of both an identification and a model-based control design criterion can be highly non-linear [2]. Although convergence and optimality of iterative schemes can not be guaranteed in general, countless numerical simulation examples presented in the literature show promising results [1,11,12,16,23].

From a practical point of view, it is valuable to monitor and guarantee performance improvement of the servo control system, while performing a step of subsequent identification and model-based control design. In this way, effort put into the steps of an iterative scheme can be justified by assuring an improvement of the feedback controlled plant.

Guaranteeing an improvement of the performance of a feedback controlled plant cannot be achieved by iteratively trying to improve nominal performance specifications alone. As the resulting model is just an approximation of the system to be identified, the controller based on the model has to be robust against any dissimilarities between the model and the system. This has been a motivation for the development of identification techniques that estimate an upper bound on the model uncertainty (model error), see for example the survey [14] and the more recent contributions [10,3]. The resulting model uncertainty bounds constitute an allowable perturbation around a nominal model being estimated and defines a set of models  $\mathcal{G}$  where the actual system  $G_0$  is assumed to be an element of. Subsequently, a robust controller can be designed on the basis of this set of models [24]. In this approach stability and performance requirements are guaranteed for the complete set of models, that includes the actual system to be controlled.

#### 3.2 Enhancement of control performance

To formalize the notion of a set of models and the characterization of robust control performance for a set of models, the following notation is considered. The notation  $G$  will be used to denote a linear time invariant system that

may represent the actual wafer stage denoted by  $G_0$  or a (nominal) model of the wafer stage denoted by  $\hat{G}$ . Furthermore, let  $\mathcal{G}$  be used to denote a set of models and  $K$  to represent a feedback controller. To indicate the progress in the iterative scheme of subsequent approximate modeling and model-based control design, the subscript  $i$  will be applied to the variables  $\hat{G}$ ,  $\mathcal{G}$  or  $K$  to indicate that the variable depends on the  $i$ th step of the iterative scheme. Finally, a control objective function is denoted by  $J(G, K)$  and the notion of control performance will be characterized by the value of a norm  $\|J(G, K)\|$ ; a smaller value of  $\|J(G, K)\|$  indicates better closed-loop control performance.

Examples of commonly used control objective functions may include mixed sensitivity, as well as LQG and IMC type of control objectives, see *e.g.*, [18]. Throughout this chapter, the control objective function  $J(G, K) \in \mathcal{RH}_\infty$  and is restricted to  $H_\infty$ -norm based performance specifications, allowing for worst-case and robust performance control design methodologies to be used.

Guaranteeing an improvement of the servo performance of a feedback controlled plant can be formalized by considering a feedback connection of the wafer stage plant  $G_0$  and a controller  $K_i$  that satisfies a performance specification  $\|J(G_0, K_i)\|_\infty \leq \gamma_i$ . To improve control performance, a new and improved controller  $K_{i+1}$  has to be designed such that the performance  $\|J(G_0, K_{i+1})\|_\infty$  satisfies

$$\|J(G_0, K_{i+1})\|_\infty \leq \gamma_{i+1} < \gamma_i. \quad (2)$$

To make the design problem in (2) tractable for an unknown plant  $G_0$ , basically two main items should be considered. Firstly a procedure must be found to access the performance  $\gamma_i$  for  $\|J(G_0, K_i)\|_\infty$  *a posteriori*, *i.e.*, when the controller  $K_i$  is implemented on the plant  $G_0$ . Secondly, the synthesis of a controller  $K_{i+1}$  must be formulated that satisfies the performance condition (2) *a priori*: before implementing the controller  $K_{i+1}$  on the plant  $G_0$ . To accomplish both aspects, a set of models  $\mathcal{G}$  will be identified and used for stability and performance robustness assessment. The following general procedure is followed.

**Procedure 1** *Let a plant  $G_0$  and an initial controller  $K_i$  form a stable feedback connection. To improve control performance undertake the following steps:*

(a) **Performance assessment by model set identification**

*Use experimental data and prior information on both the data and the plant  $G_0$  to estimate a set of models  $\mathcal{G}_i$  such that  $G_0 \in \mathcal{G}_i$  and determine*

$$\gamma_i = \sup_{G \in \mathcal{G}_i} \|J(G, K_i)\|_\infty. \quad (3)$$

*Subsequently, consider the following subsequent steps for performance robustness improvement of the feedback controlled plant  $G_0$ :*

**(b) Robust control design on the basis of identified model set**

Design a new controller  $K_{i+1}$  such that

$$\|J(G, K_{i+1})\|_\infty \leq \gamma_{i+1} < \gamma_i \quad \forall G \in \mathcal{G}_i \quad (4)$$

and, when achieved, implement the controller.

**(c) Validate robust controller and identify a new model set**

Use (new) experimental data and prior information on both the data and the plant  $G_0$  to estimate a set of models  $\mathcal{G}_{i+1}$  such that  $G_0 \in \mathcal{G}_{i+1}$  and

$$\|J(G, K_{i+1})\|_\infty \leq \gamma_{i+1} \quad \forall G \in \mathcal{G}_{i+1}. \quad (5)$$

The formulation of Procedure 1 is a rather general set-up to generate a sequence of model-based controllers that will satisfy (2). Within this set-up, step (b) reflects the design of a robust controller in order to ensure (2). Both step (a) and (c) contain the estimation of a set of models  $\mathcal{G}$ . These steps will constitute an identification problem to estimate the set  $\mathcal{G}$  and/or a model (in)validation problem [17] in order to guarantee  $G_0 \in \mathcal{G}$ . However, both the identification problem and the model (in)validation problem should be control relevant. This is reflected by the fact that the quality of the models  $G$  within a set  $\mathcal{G}$  is evaluated by the performance specification  $\|J(G, K)\|_\infty$ , where step (a) and (c) differ only in the feedback controller  $K$  being used.

By iterating on the subsequent steps (b) and (c), an iterative scheme of identification and control is formulated, where (4) and (5) reflect respectively a controller and a model closed-loop *validation test* in order to enforce (2). Starting from step (a), where  $K_i$  is the controller (initially) implemented on the plant  $G_0$ , (3) can be viewed as an initial closed-loop performance assessment test to evaluate  $\|J(G_0, K_i)\|_\infty$  *a posteriori*. In the robust control design of step (b), Equation 4 is needed to ensure (2) *a priori*. In this way, both performance robustness and improvement of the upper bound on the closed-loop performance can be guaranteed for  $K_{i+1}$ . The performance  $\|J(G_0, K_i)\|_\infty$  can be evaluated *a posteriori*, by implementation of  $K_{i+1}$  on the plant  $G_0$  and estimating a new set  $\mathcal{G}_{i+1}$ . If indeed (5) is satisfied, in step (b) again a new controller can be designed on the basis of  $\mathcal{G}_{i+1}$ .

Although the problem formulation in Procedure 1 is fairly general and somehow trivial, it does provide a monotonic non-decreasing sequence of  $\gamma_i$ . A similar idea was proposed in [2]. Obviously, to provide a feasible procedure for handling Procedure 1, the choice for the structure of the set of models  $\mathcal{G}$  should be addressed [19].

Summarizing, the following items will play an important role in the realization of an iterative scheme as proposed here:

- The control objective function  $J(G, K)$ . The objective function plays a crucial role in the characterization of performance robustness and the way in which a controller is designed.

- Evaluation of the closed-loop performance (3) and the closed-loop validation test of (4) and (5) in a non-conservative way. A proper choice for the structure of the set of models  $\mathcal{G}$  will benefit the evaluation of the performance robustness.
- Identification procedure to estimate a set of models  $\mathcal{G}$ . Similar procedures are needed in step (a) and (c) by considering respectively the feedback controllers  $K_i$  and  $K_{i+1}$  and the estimation procedure should take into account the control design application of the set  $\mathcal{G}$ .
- Robust control design method. The design of a controller on the basis of a set of models  $\mathcal{G}$  in step (b) is needed to ensure (2).

In the remaining part of this chapter, the iterative scheme of model set estimation and robust control design will be described and applied to the motion control system of the wafer stage. The items mentioned above will be outlined in separate sections to clearly indicate the different aspects.

## 4 Elements of the Iterative Scheme

### 4.1 Performance and control objective

The mapping from the reference signals  $(r_2, r_1)$  to the output and input signals  $(y, u)$  of the plant in Figure 4 is given by the transfer function matrix  $T(G_0, K_i)$  with

$$T(G_0, K_i) := \begin{bmatrix} G_0 \\ I \end{bmatrix} (I + K_i G_0)^{-1} \begin{bmatrix} K_i & I \end{bmatrix}. \quad (6)$$

As a result, the data obtained from the feedback connection  $\mathcal{T}(G_0, K_i)$  of Figure 4 can be described by

$$\begin{bmatrix} y \\ u \end{bmatrix} = T(G_0, K_i) \begin{bmatrix} r_2 \\ r_1 \end{bmatrix} + \begin{bmatrix} I \\ -K_i \end{bmatrix} (I + G_0 K_i)^{-1} v. \quad (7)$$

The transfer function matrix  $T(G_0, K_i)$  characterizes all closed-loop properties of a feedback connection of plant  $G_0$  and controller  $K_i$ . Note that a feedback connection  $\mathcal{T}(G, K)$  is internally stable if and only if  $T(G, K)$  is stable.

In order to incorporate control design specification for the map  $T(G, K)$ , the control objective function  $J(G, K)$  is taken to be a weighted form of the matrix  $T(G, K)$  given in (6) and is defined as

$$\|J(G, K)\|_\infty := \|U_2 T(G, K) U_1\|_\infty \quad (8)$$

where  $U_2$  and  $U_1$  are (square) weighting functions. These weighting functions are chosen in such a way that the bandwidth of the resulting feedback connection can be adjusted, which will increase the speed of decay of the resulting servo error depicted in Figure 6. Furthermore, the weighting functions can

be used to design a controller  $K$  that allows for an additional suppression of the low frequent vibration of the servo error.

In this particular situation the weighting functions are chosen to comply with a loop shaped situation. By choosing:

$$U_2 = \begin{bmatrix} U_l & 0 \\ 0 & U_r^{-1} \end{bmatrix} \quad U_1 = U_2^{-1}$$

the performance objective function  $J$  can be written as

$$J(G, K) = \begin{bmatrix} U_l G \\ U_r^{-1} I \end{bmatrix} [I + KG]^{-1} [KU_l^{-1} \quad U_r] \quad (9)$$

$$= T(G_{ls}, K_{ls}) \quad (10)$$

with  $G_{ls} = U_l G U_r$  and  $K = U_r K_{ls} U_l$ .

The performance characterization (8) is fairly general and will be used for analyzing performance robustness and designing servo controllers for the wafer stage.

## 4.2 Set of models and evaluation of performance robustness

The characterization of a set of models allows one to capture the actual system  $G_0 \in \mathcal{G}$ . In this way performance robustness can be monitored via a worst-case performance evaluation over the set of models  $\mathcal{G}$ , whereas performance robustness can be enforced via a robust controller design.

Employing the knowledge of the stabilizing controller  $K_i$ , a set of models  $\mathcal{G}_i$  can be characterized by using the algebraic theory of fractional model representations [21]. The uncertainty structure used in our procedure is based on a dual-Youla parametrization:

$$\mathcal{G}_i = \{G \mid G = (\hat{N} + D_k \Delta)(\hat{D} - N_k \Delta)^{-1}, \\ \text{with } \Delta \in \mathcal{RH}_\infty \text{ and } \|\hat{V} \Delta \hat{W}\|_\infty < \gamma_i^{-1}\} \quad (11)$$

where  $(N_k, D_k)$  denotes a right coprime factorization (*ref*) of the controller  $K_i$  implemented on the plant  $G_0$  during closed-loop experiments. Similarly,  $(\hat{N}, \hat{D})$  denotes a *ref* of a nominal model  $\hat{G}_i$  of the plant  $G_0$  that satisfies  $T(\hat{G}_i, K_i) \in \mathcal{RH}_\infty$ . The (stable and stably invertible) weighting functions  $\hat{V}$ ,  $\hat{W}$  are used to normalize the upper bound on  $\hat{V} \Delta \hat{W}$  to  $\gamma_i^{-1}$ . A schematic representation of the uncertainty structure is depicted in Figure 8.

The uncertainty structure in (11) has several attractive properties that makes it useful for closed-loop identification and worst-case performance analysis:

- All models  $G \in \mathcal{G}_i$ , including the unknown plant  $G_0$  are guaranteed to be stabilized by the current controller  $K_i$ . This property indicates that the dual-Youla based set of models exploits the information that the actual plant  $G_0$  has been stabilized by the controller  $K_i$  during the closed-loop experiments.

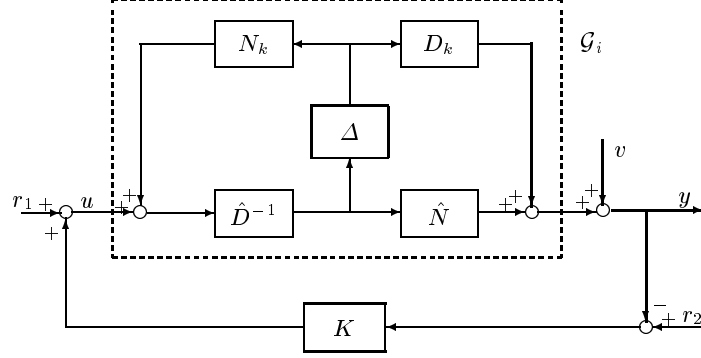


**Fig. 8.** Block scheme of dual-Youla based uncertainty structure of models  $G \in \mathcal{G}_i$  operating in closed-loop with a controller  $K$

- The calculation of the worst-case performance of a controller  $K$  over all models  $G \in \mathcal{G}_i$  can be done relatively easy. In fact, the worst-case performance criterion reduces to an affine expression in  $\Delta$  if the worst-case performance needs to be evaluated for the controller  $K_i$ , also used in characterizing the model set  $\mathcal{G}_i$  in (11).
- The uncertainty term  $\Delta$  is accessible from closed-loop data. This will be utilized in actual estimation of an upper bound for the uncertainty on the basis of closed-loop experiments.

In order to explain the favorable properties listed above, a Linear Fractional Transformation (LFT) description of the set  $\mathcal{G}_i$  in (11) is used to simplify the algebraic manipulations. An (upper) LFT  $\mathcal{F}_u(Q, \Delta)$  is defined by

$$\mathcal{F}_u(Q, \Delta) := Q_{22} + Q_{21}\Delta(I - Q_{11}\Delta)^{-1}Q_{12} \quad (12)$$

provided that  $(I - Q_{11}\Delta)^{-1}$  exists. The set of models  $\mathcal{G}_i$  in (11) can then be characterized by

$$\mathcal{G}_i = \{G \mid G = \mathcal{F}_u(Q_i, \Delta), \text{ with } \Delta \in \mathcal{RH}_\infty \text{ and } \|\Delta\|_\infty < \gamma_i^{-1}\}$$

where  $\Delta$  indicates the same unknown (but bounded) uncertainty as in (11). The entries of the coefficient matrix  $Q_i$  in (12) dictate the way in which the set of models  $\mathcal{G}$  is being structured. For the set  $\mathcal{G}_i$  in (11) it can be verified that the entries of  $Q_i$  are given by

$$Q_i = \begin{bmatrix} \hat{W} & 0 \\ 0 & I \end{bmatrix} \left[ \begin{array}{c|c} \hat{D}^{-1}N_k & \hat{D}^{-1} \\ \hline (D_k + \hat{G}_iN_k) & \hat{G} \end{array} \right] \begin{bmatrix} \hat{V}^{-1} & 0 \\ 0 & I \end{bmatrix}. \quad (13)$$

As a special entry one can recognize the nominal model  $\hat{G}_i = \mathcal{F}(Q_i, 0) = Q_{22}$ .

Since  $\mathcal{G}_i$  is characterized by an LFT, the connection between any controller  $K$  and the set of models  $\mathcal{G}_i$  can also be characterized by an LFT, thus enabling a relatively simple calculation of worst-case performance when  $K$  is applied to all models within  $\mathcal{G}_i$ . It appears that for all models  $G \in \mathcal{G}_i$  the control objective function  $J(G, K)$  can be written as

$$J(G, K) = \mathcal{F}_u(M_i, \Delta)$$

with the entries of  $M_i$  given by (see [8]):

$$\begin{aligned} M_{11} &= -\hat{W}^{-1}(\hat{D} + K\hat{N})^{-1}(K - K_i)D_k\hat{V}^{-1} \\ M_{12} &= \hat{W}^{-1}(\hat{D} + K\hat{N})^{-1} [K \ I] U_1 \\ M_{21} &= -U_2 \begin{bmatrix} -I \\ K \end{bmatrix} (I + \hat{G}_i K)^{-1} (I + \hat{G}_i K_i) D_k \hat{V}^{-1} \\ M_{22} &= U_2 \begin{bmatrix} \hat{N} \\ \hat{D} \end{bmatrix} (\hat{D} + K\hat{N})^{-1} [K \ I] U_1. \end{aligned} \quad (14)$$

Note that in this formulation the controller  $K$  can be given by either the present controller  $K = K_i$  referring to the situation of *posterior stability/performance assessment*, or by a newly designed controller  $K = K_{i+1}$ , related to a *prior stability/performance robustness test*.

The entry  $M_{11}$  plays an important role in stability robustness analysis of a controller  $K$  applied to all models in the model set. For  $K = K_i$ ,  $M_{11} = 0$  implying that all controller/model pairs resulting from  $\mathcal{G}_i$  are stable, irrespective of the size of  $\Delta$ . This property of the dual-Youla parametrization has been indicated before. For  $K = K_{i+1}$ , stability robustness can be guaranteed by verifying if  $\|M_{11}\|_\infty < \gamma_i$ . This pertains to a test on a *lower* LFT:  $\|\mathcal{F}_l(Q_i, -K)\|_\infty < \gamma_i$  (see [8]).

For performance evaluation we distinguish again between the *posterior* and the *prior* situation.

- **Performance assessment for implemented controller.**

For posterior performance assessment (step (a) of the procedure), we have  $K = K_i$ , and the worst-case performance  $\|J(G, K_i)\|_\infty$  over all models  $G \in \mathcal{G}_i$  is evaluated by calculating

$$\|\mathcal{F}_u(M_i, \Delta)\|_\infty = \|M_{22} + M_{21}\Delta M_{12}\|_\infty$$

for all  $\Delta \in \mathcal{RH}_\infty$  with  $\|\Delta\|_\infty \leq \gamma_i^{-1}$ . This test can be performed non-conservatively.

- **Robust performance test for designed -not yet implemented- controller.**

For a prior performance robustness test (step (b) of the procedure), we have  $K = K_{i+1}$ , and the necessary evaluation becomes

$$\|\mathcal{F}_u(M_i, \Delta)\|_\infty = \|M_{22} + M_{21}\Delta(I - M_{11}\Delta)^{-1}M_{12}\|_\infty \leq \gamma_i^{-1} \quad (15)$$

for all  $\Delta \in \mathcal{RH}_\infty$  with  $\|\Delta\|_\infty \leq \gamma_i^{-1}$ . Note that evaluation of (15) can be done via the application of the main loop theorem and by computing an upper bound for the structured singular value of  $\mu(M_i)$ , see *e.g.*, theorem 11.7 in [24]. With the result of the main loop theorem,  $\mathcal{F}_u(M_i, \Delta)$  is well-posed, stable and  $\|\mathcal{F}_u(M_i, \Delta)\|_\infty \leq \gamma_i^{-1}$  for all  $\Delta$  with  $\|\Delta\|_\infty < \gamma_i^{-1}$ , if and only if

$$\mu(M_i) \leq \gamma_i \quad (16)$$

where the structured singular value  $\mu(M_i)$  is computed with respect to the block diagonal structure of  $M_i$  given in (14).

For step (c) of the procedure the prior performance assessment test is used similar to the situation of step (a), albeit now with the *known* controller  $K_{i+1}$ , and an updated  $M_{i+1}$ .

### 4.3 Control relevant estimation of a set of models

As indicated in (11), the structure of a set of models  $\mathcal{G}$  is determined by a *rcf*  $(\hat{N}, \hat{D})$  of a nominal model  $\hat{G}$  and the weighting functions  $(\hat{V}, \hat{W})$  that normalize the uncertainty or modeling error. The control relevant estimation of a set of models  $\mathcal{G}$  should address the minimization

$$(\hat{N}, \hat{D}, \hat{V}, \hat{W}) = \arg \min_{N, D, V, W} \sup_{G \in \mathcal{G}} \|J(G, K)\|_\infty \quad (17)$$

subjected to both  $G_0 \in \mathcal{G}$  and internal stability of the feedback connection  $\mathcal{T}(\hat{G}, K)$ . At the current state, the minimization of (17) using the variables  $(\hat{N}, \hat{D}, \hat{V}, \hat{W})$  simultaneously, cannot be solved directly. Therefore, the control relevant identification of a set of models in (17) is addressed by estimating the *rcf*  $(\hat{N}, \hat{D})$  and the pair  $(\hat{V}, \hat{W})$  separately:

- *Estimation of a nominal model*

This involves the estimation of  $\hat{G} = \hat{N}\hat{D}^{-1}$  such that (17) is being minimized using the *rcf*  $(N, D)$  only, subjected to internal stability of  $\mathcal{T}(\hat{G}, K)$ . The pair  $(\hat{V}, \hat{W})$  is unknown and assumed to vary freely in order to satisfy  $G_0 \in \mathcal{G}$ .

- *Estimation of uncertainty*

This consists of the characterization of an upper bound on  $\Delta$  in (11) via  $(\hat{V}, \hat{W})$  such that (17) is being minimized using  $(V, W)$  only, subjected to  $G_0 \in \mathcal{G}$ . The *rcf*  $(\hat{N}, \hat{D})$  is fixed to the estimate of the nominal model obtained previously.

By the separate identification of the *rcf*  $(\hat{N}, \hat{D})$  and the weighting functions  $(\hat{V}, \hat{W})$  only an upper bound on (17) can be minimized. However, it should be stressed that precise minimization of (17) is not needed. It suffices to find a set of models that passes the *a posteriori* performance robustness test of

(3) or (5). Furthermore, (standard) tools to estimate a nominal model and to characterize uncertainty can be applied as indicated in the application to the wafer stage. Finally it can be noted that due to the separation being made, the attention can be focused on finding models of limited complexity [18]. The rationale is to avoid the computation of controllers on the basis of highly complex models as much as possible, since this will lead to high-order controllers for which the computation may be badly conditioned.

#### 4.4 Robust control design

A new and improved robust performing controller controller  $K_{i+1}$  can be designed on the basis of the estimated set of models  $\mathcal{G}_i$  by the minimization

$$K_{i+1} = \arg \min_K \sup_{G \in \mathcal{G}_i} \|J(G, K)\|_\infty. \quad (18)$$

Basically, (18) is a robust performance control design, wherein a controller  $K_{i+1}$  is constructed such that the worst case performance  $J(G, K_{i+1})$  for all  $G \in \mathcal{G}_i$  is being optimized. In order to use the available standard results on  $\mathcal{H}_\infty$ - and  $\mu$ -controller synthesis, the transfer function  $M_i$  of the LFT  $\mathcal{F}_u(M_i, \Delta)$  in (14) is represented as a lower fractional transformation  $\mathcal{F}_l(P_i, K)$  as illustrated in Figure 9.

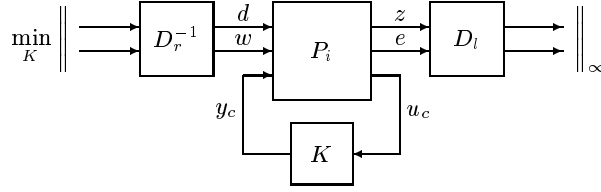


**Fig. 9.** Controller synthesis via  $\mathcal{H}_\infty$  optimization for fixed  $D$ -scaling

The entries of the standard plant  $P_i$  in Figure 9 can be found by extracting the controller  $K$  from the expression of  $M_i$  given in (14). Considering the map  $M_i$  given in (14), then  $M_i = \mathcal{F}_l(P_i, K)$  where  $P_i$  is given by

$$P_i = \begin{bmatrix} \hat{W}^{-1} & 0 & 0 \\ 0 & U_2 & 0 \\ 0 & 0 & I \end{bmatrix} \left[ \begin{array}{c|c|c} \hat{D}^{-1} N_k & \hat{D}^{-1} 0 & \hat{D}^{-1} \\ \hline (D_k + \hat{G}_i N_k) & \hat{G}_i & 0 \\ \hline 0 & I & 0 \\ \hline -(D_k + \hat{G}_i N_k) & -\hat{G}_i & I \end{array} \right] \begin{bmatrix} -\hat{V}^{-1} & 0 & 0 \\ 0 & U_1 & 0 \\ 0 & 0 & I \end{bmatrix}.$$

The control design problem (18) can be tackled via a  $\mu$ -synthesis that solves

$$\min_K \inf_{D_l, D_r \in \mathcal{D}} \|D_l \mathcal{F}_l(P_i, K) D_r^{-1}\|_\infty \quad (19)$$

iteratively for the scaling matrices  $D_l$ ,  $D_r$  and the controller  $K$ , subjected to internal stability of the feedback connection of  $K$  and  $\hat{G}_i$ .

Finally it can be noted that the control design used here is a generalization of the robust controller synthesis as presented in *e.g.*, [4] or [13]. It can be verified that by ignoring the map from  $d$  onto  $z$  (representing the uncertainty),  $P$  reduces to

$$\begin{bmatrix} U_2 & 0 \\ 0 & I \end{bmatrix} \left[ \begin{array}{c|c} \hat{G}_i & 0 \\ \hline I & 0 \\ \hline -\hat{G}_i & I \end{array} \right] \begin{bmatrix} U_1 & 0 \\ 0 & I \end{bmatrix}$$

and  $M_i = \mathcal{F}_l(P_i, K) = U_2 T(\hat{G}_i, K) U_1$ . In the special case of a *diagonal* weighting function  $U = \text{diag}(U_{in}, U_{out}^{-1})$  with  $U_2 = U$  and  $U_1 = U^{-1}$ , the controller  $K_{i+1}$  that minimizes  $\|UT(\hat{G}_i, K_{i+1})U^{-1}\|_\infty$  can be found by loop shaping techniques [4, pp. 107-108]. Explicit state space formulae of the optimal controller for this special case can be found in [4] or [13].

## 5 Estimation of Model Set for the Wafer Stage

### 5.1 Access to coprime factorizations

The first step in the characterization of the set of models  $\mathcal{G}$ , is the (approximate) identification of a stable nominal factorization  $(\hat{N}, \hat{D})$  of a (possibly unstable) nominal model  $\hat{G}$ . Access to a *rcf* of the system  $G_0$  for identification purposes can be obtained by a simple filtering of the signals present in the feedback connection  $\mathcal{T}(G_0, K_i)$ .

As indicated in [20] or [7], a filtering of the reference signal  $r := r_1 + K_i r_2 = u + K_i y$  via  $x := Fr$  enables access to the various *rcf* of the system  $G_0$  on the basis of closed-loop data. With (7) it can be seen that

$$x = F \begin{bmatrix} K_i & I \end{bmatrix} \begin{bmatrix} r_2 \\ r_1 \end{bmatrix} = F \begin{bmatrix} K_i & I \end{bmatrix} \begin{bmatrix} y \\ u \end{bmatrix} \quad (20)$$

and (7) reduces to

$$\begin{bmatrix} y \\ u \end{bmatrix} = \begin{bmatrix} G_0 S_{in} F^{-1} \\ S_{in} F^{-1} \end{bmatrix} x + \begin{bmatrix} (I + G_0 K_i)^{-1} \\ -K_i (I + G_0 K_i)^{-1} \end{bmatrix} v \quad (21)$$

where  $(G_0 S_{in} F^{-1}, S_{in} F^{-1})$  with  $S_{in} = (I + K_i G_0)^{-1}$  can be considered to be a (right) factorization of the system  $G_0$ . In order for this factorization to be right coprime, the filter  $F$  in (20) is restricted to the form

$$F = [D_x + K_i N_x]^{-1} \quad (22)$$

where  $(N_x, D_x)$  is a *rcf* of any auxiliary model  $G_x$  that is stabilized by the (initial) controller  $K_i$  used in the closed-loop experiments. For more details on this characterization, see [20]. This includes choices for  $F$  that achieve

normalization of the factorization  $(N_{o,F}, D_{o,F})$  which has the additional advantage that redundant dynamics in the two factors is removed.

Consequently, a simple filtering (20) of the signals present in the feedback connection  $\mathcal{T}(G_0, K_i)$  allows the access to a *rcf* of the system  $G_0$ . The system equation (7) can then be written in the form

$$\begin{bmatrix} y \\ u \end{bmatrix} = \begin{bmatrix} N_{o,F} \\ D_{o,F} \end{bmatrix} x + \begin{bmatrix} I \\ -K_i \end{bmatrix} [I + G_0 K_i]^{-1} v \quad (23)$$

where  $x$  is given in (20),  $F$  is given in (22) and  $(N_{o,F}, D_{o,F})$  is the *rcf* of the plant  $G_0$  given by

$$\begin{bmatrix} N_{o,F} \\ D_{o,F} \end{bmatrix} = \begin{bmatrix} G_0 \\ I \end{bmatrix} [I + K_i G_0]^{-1} [I + K_i G_x] D_x. \quad (24)$$

Since  $x$  in (20) is uncorrelated with  $v$ , (23) gives rise to an equivalent open loop identification problem of the *rcf*  $(N_{o,F}, D_{o,F})$  of the system  $G_0$ .

## 5.2 Feedback relevant estimation of coprime factorizations

In the estimation of the *rcf*  $(\hat{N}, \hat{D})$ , minimization of (17) must be taken into account when estimating a nominal factorization  $(\hat{N}, \hat{D})$ . Furthermore,  $\hat{G} = \hat{N}\hat{D}^{-1}$  is subjected to internal stability of the feedback connection  $\mathcal{T}(\hat{G}, K_i)$  in order to characterize the set of models  $\mathcal{G}$  given in (11).

Clearly, at this stage the set of models is unknown and (17) cannot be computed. In fact, the set of models is arbitrarily large as the norm bounded uncertainty  $\Delta$  in (11) has not been characterized. Consequently, for any nominal model there exists a norm bounded uncertainty  $\Delta$  that forms a set of models  $\mathcal{G}$  for which  $G_0 \in \mathcal{G}$ . As  $G_0 \in \mathcal{G}$ , for any nominal model  $G_0 \in \mathcal{G}$  the following upper bound for  $\|J(\hat{G}, K_i)\|_\infty$  can be given.

$$\|J(\hat{G}, K_i)\|_\infty \leq \|J(G_0, K_i)\|_\infty + \|J(\hat{G}, K_i) - J(G_0, K_i)\|_\infty$$

As  $\|J(G_0, K_i)\|_\infty$  in the above expression does not depend on the nominal model  $\hat{G}$ , the upper bound can be minimized by an estimated *rcf*  $(\hat{N}, \hat{D})$  of a nominal model that minimizes

$$\|J(\hat{G}, K_i) - J(G_0, K_i)\|_\infty \quad (25)$$

thus constituting a control-relevant identification criterion.

With the expressions introduced above, it can be shown [7] that

$$J(G_0, K_i) - J(\hat{G}, K_i) = U_2 \left( \begin{bmatrix} N_{o,F} \\ D_{o,F} \end{bmatrix} - \begin{bmatrix} \hat{N} \\ \hat{D} \end{bmatrix} \right) F [K_i \ I] U_1 \quad (26)$$

where  $(\hat{N}, \hat{D})$  satisfies the constraint  $\hat{D} + K_i \hat{N} = F^{-1}$ . The estimation of a nominal factorization for the positioning mechanism of the wafer stepper will be illustrated in the next section.

### 5.3 Estimation results of nominal factorizations

To estimate a nominal factorization  $(\hat{N}, \hat{D})$ , frequency domain measurements of the factorization  $N_{o,F}(\omega)$ ,  $D_{o,F}(\omega)$  along a prespecified frequency grid are used. The external signals  $r_1$  and  $r_2$  are designed accordingly to the experiment design discussed in Section 2.4.

Subsequently, the curve fitting procedure described in [6] is used to tackle the weighted minimization of (25) frequency wise. As the curve fitting procedure is a non-linear optimization, an initial estimate is required to start the optimization. For that purpose, a multivariable least squares curve fitting procedure is used [5].

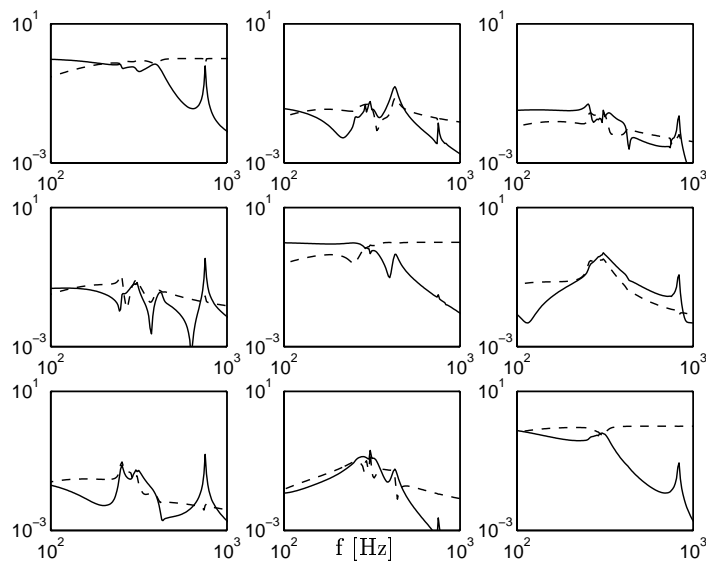
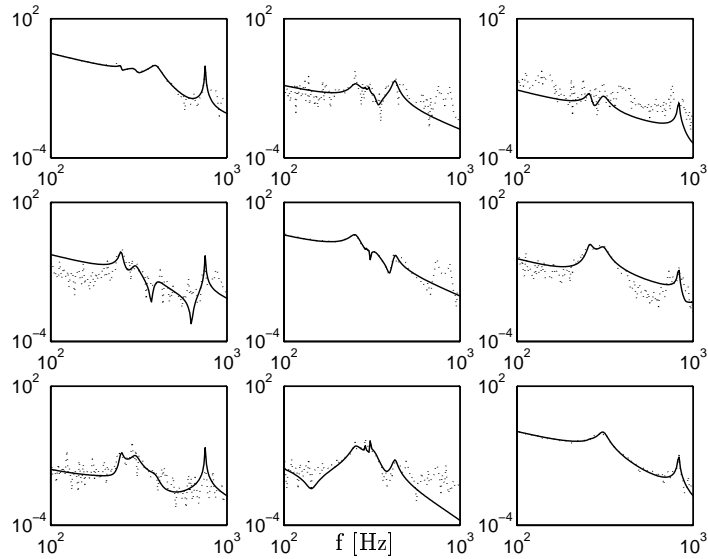


Fig. 10. Amplitude Bode plot of estimated coprime factors  $\hat{N}$  (—) and  $\hat{D}$  (- -)

An amplitude Bode plot of the *rcf*  $(\hat{N}, \hat{D})$  being estimated can be found in Figure 10. The resulting estimate of  $col(\hat{N}, \hat{D})$  is an 18th-order discrete time multivariable model having 6 inputs and 3 outputs. Computing  $\hat{G}_i = \hat{N}\hat{D}^{-1}$  yields a 18th-order nominal model, having 3 inputs and 3 outputs. The amplitude Bode plot of the model  $\hat{G}_i$ , along with the available frequency domain data computed via  $N_{o,F}(\omega)D_{o,F}(\omega)^{-1}$  is depicted in Figure 11.

Although stability of the feedback connection  $\mathcal{T}(\hat{G}_i, K_i)$  is not enforced during the estimation of the coprime factorization  $(\hat{N}, \hat{D})$ , the model  $\hat{G}_i$  is stabilized by  $K_i$ . This is mainly due to the fact that the control-relevant estimation of the coprime factors yields a nominal model  $\hat{G}_i$  with a good



**Fig. 11.** Amplitude Bode plot of computed nominal model  $\hat{G}_i$  (—) and frequency domain data ( $\dots$ )

fit of the control relevant dynamical behavior of the plant  $G_0$  around the closed-loop relevant frequency area of 200Hz.

With the knowledge of the 18th-order curve-fitted nominal plant model  $\hat{G}_i$ , the weighting functions  $U_1$  and  $U_2$  for the control objective function  $J(G, K)$  are designed. They are chosen to achieve decoupling of the multi-variable plant at 90 Hz and to achieve a nominal bandwidth of approximately 90 Hz. Furthermore 2 integrators are incorporated in each diagonal transfer of the loop-shaped plant to ensure low frequent disturbance rejection and tracking of the servo positioning mechanism.

#### 5.4 Access to model uncertainty

Once a *rcf*  $(\hat{N}, \hat{D})$  of the nominal model  $\hat{G}_i$  is obtained, an estimation of the model(ling) uncertainty  $\Delta$  in (11) can be performed. This involves the characterization of an upper bound on  $\Delta$  in (11) via the stable and stably invertible filters  $(\hat{V}, \hat{W})$  such that (17) is being minimized and  $G_0 \in \mathcal{G}_i$ . For that purpose, first (an upper bound on) the allowable model perturbation  $\Delta$  is determined by applying a model error bounding estimation technique. The uncertainty estimation routine described by [9] is used to obtain a frequency dependent upper bound for  $\Delta$

$$\|\Delta(\omega)\| \leq \delta(\omega) \text{ with probability } \geq \alpha \quad (27)$$

where  $\alpha$  is a pre-chosen probability. In the multivariable case, the upper bound (27) can be obtained for each transfer function. Subsequently, stable and stably invertible weightings  $\hat{V}$  and  $\hat{W}$  can be determined that overbound the estimated upper bound  $\delta(\omega)$ .

In order to estimate a frequency dependent upper bound on  $\Delta$ , the map  $\Delta$  must be accessible from data. This can be achieved by defining the filtered closed-loop signal

$$z := (D_k + \hat{G}_i N_k)^{-1} [I - \hat{G}_i] \begin{bmatrix} y \\ u \end{bmatrix} \quad (28)$$

which can be shown to satisfy

$$z = \Delta x + D_k (I + G_0 K_i)^{-1} v. \quad (29)$$

As  $x$  is uncorrelated with  $v$  this points to an open loop bounded error identification problem to find an upper bound for a stable  $\Delta$ . The estimated upper bound of  $\Delta$  in (27) can then be used to complete the characterization of the set of models  $\mathcal{G}_i$ .

### 5.5 Feedback relevant estimation of model uncertainty

It can be observed from (14) that knowledge of the controller  $K_i$  used during the closed-loop experiments is taken into account in the construction of the set of models. Application of the same controller  $K = K_i$  to the uncertainty set for a *posteriori* robust performance evaluation greatly reduces the entries of the matrix  $M$ . Substitution of  $K = K_i$  in (14) yields  $M_{11} = 0$ . This implies that when the controller  $K_i$  is applied to the estimated set of models  $\mathcal{G}_i$ , the upper LFT  $\mathcal{F}_u(M, \Delta)$  modifies into

$$M_{22} + M_{21} \Delta M_{12} \quad (30)$$

which is an affine expression in  $\Delta$ .

Substituting  $M_{21}$  and  $M_{12}$  in (30) with  $\Delta = \hat{V} \Delta \hat{W}$  yields the following expression

$$M_{22} + M_{21} \Delta M_{12} = M_{22} + W_2 \Delta W_1$$

where

$$W_2 = -U_2 \begin{bmatrix} -D_k \\ N_k \end{bmatrix}, \quad W_1 = \hat{D}^{-1} (I + K_i \hat{G}_i)^{-1} [K_i \ I] U_1. \quad (31)$$

Consequently, the effect of replacing an accurate (and high-order estimate) of the upper bound  $\Delta$  by a low-order upper bound approximation  $\tilde{\Delta}$  on the (robust) performance  $\|J(G_0, K_i)\| = \|M_{22} + W_2 \Delta W_1\|$  can be bounded by the following triangular inequality

$$\|M_{22} + W_2 \Delta W_1\| \leq \|M_{22} + W_2 \tilde{\Delta} W_1\| + \|W_2 (\Delta - \tilde{\Delta}) W_1\| \quad (32)$$

From (32) it can be observed that, similar to identification of a control relevant and low complexity factorization of a nominal model, a weighted difference between the actual and highly complex uncertainty  $\Delta$  and the low complexity approximation  $\tilde{\Delta}$  must be taken into account for a control relevant approximation of the model uncertainty. The weightings  $W_2$  and  $W_1$  are given in (31) and are known, once a nominal factorization  $(\hat{N}, \hat{D})$  has been estimated. With the (frequency dependent) weightings  $W_1$  and  $W_2$ , low frequent weighting filters  $(\hat{V}, \hat{W})$  can be used to parametrize and overbound the frequency dependent bound of the modeling uncertainty.

## 5.6 Estimation results of model uncertainty

Given the nominal factorization  $(\hat{N}, \hat{D})$  and a normalized *rcf*  $(N_k, D_k)$  of the controller  $K_i$ , an estimation of the allowable model perturbation  $\Delta$  in (11) is performed. For that purpose, the uncertainty estimation as presented in [9] has been applied to estimate a frequency dependent upper bound on  $\Delta$ . A complete discussion on the uncertainty estimation procedure of [9] is beyond the scope of this paper. Here we will just point to its main characteristics:

- it combines a worst-case bounding of unmodelled dynamics with a probabilistic bound on the variance error;
- it employs linearly parametrized models (basis functions) for which least-squares or IV estimates are constructed;
- uncertainty regions for frequencies in any user-chosen frequency grid are computed from bias and variance errors.

The result of the uncertainty bounding procedure is summarized in Figure 12. In Figure 12 the amplitude bodeplot of the frequency domain data of  $\Delta$  in (29) is compared with the estimated upper bound  $\delta(\omega)$ . It can be observed from Figure 12 that the upper bound of the frequency domain estimation of  $\Delta$  is crossing the upper bound  $\delta(\omega)$ . Partly, this is due to the fact the upper bound only holds within a prespecified probability of 95%.

As  $\delta(\omega)$  is only a frequency dependent upper bound for  $\Delta$ , low frequent weighting filters  $(\hat{V}, \hat{W})$  are needed to parametrize and overbound the estimated uncertainty bound  $\delta(\omega)$  depicted in Figure 12. In this way, the estimated upper bound can be taken into account during a robust controller design.

In the construction of  $(\hat{V}, \hat{W})$  the weightings  $W_1$  and  $W_2$  given in (31) are used to emphasize the frequency range for the upper bounding of  $\delta(\omega)$  by the parametric stable and stably invertible weightings  $(\hat{V}, \hat{W})$ . It can be observed from (31) that the input sensitivity  $(I + K_i \hat{G}_i)^{-1}$ , based on the nominal model  $\hat{G}_i$ , is incorporated in the weightings given in (31). As a consequence, the weightings emphasize (again) the closed-loop relevant frequency area around 200Hz.

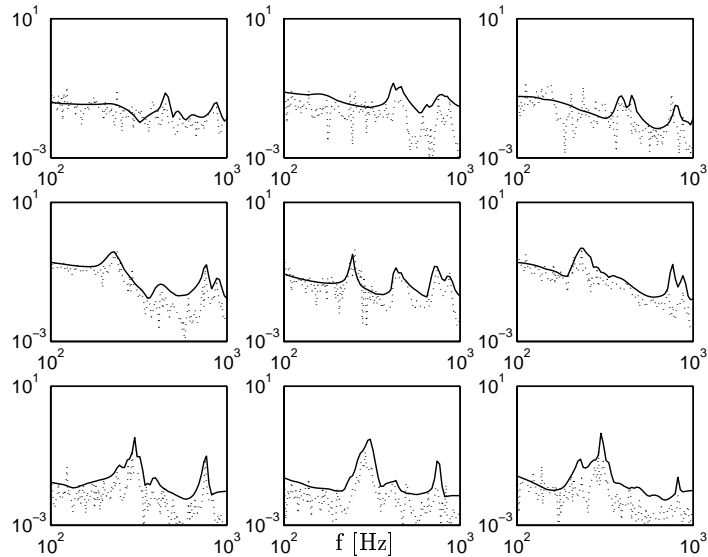


**Fig. 12.** Amplitude Bode plot of estimated uncertainty bound  $\delta(\omega)$  (—) of  $\Delta$  and frequency domain estimate of  $\Delta$  (···)

## 6 Model Set Based Robust Control Design

On the basis of the identified set of models, a robust controller can be designed via a  $\mu$ -synthesis. As indicated in Section 4.4, a robust performance control design is used wherein a controller  $K_{i+1}$  is constructed such that the worst case performance  $J(G, K_{i+1})$  for all  $G \in \mathcal{G}_i$  is being optimized. The control design is done via a  $\mu$ -synthesis using an alternating iteration between a  $\mathcal{H}_\infty$  controller optimization with fixed D scalings and an adjustment of the scalings  $D$  for a fixed controller.

The  $\mu$ -synthesis is invoked with 2nd-order  $D$ -scalings and four D-K iterations are performed to compute a robust performing controller. The  $\mu$ -synthesis yields a high-order multivariable feedback controller and in order to implement the controller, an additional closed-loop controller reduction [22] was used to reduce the controller to a 32nd-order state space realization. A comparison between the initial controller  $K_i$  previously implemented on the wafer stage system and the newly designed controller  $K_{i+1}$  is given in terms of the amplitude Bode plot depicted in Figure 13.

Compared to the initial controller  $K_i$  it can be seen that the newly designed  $K_{i+1}$  is a multivariable servo controller. Furthermore it has additional dynamics to account for the modelled (uncertain) mechanical resonance modes of the wafer stage  $G_0$ .

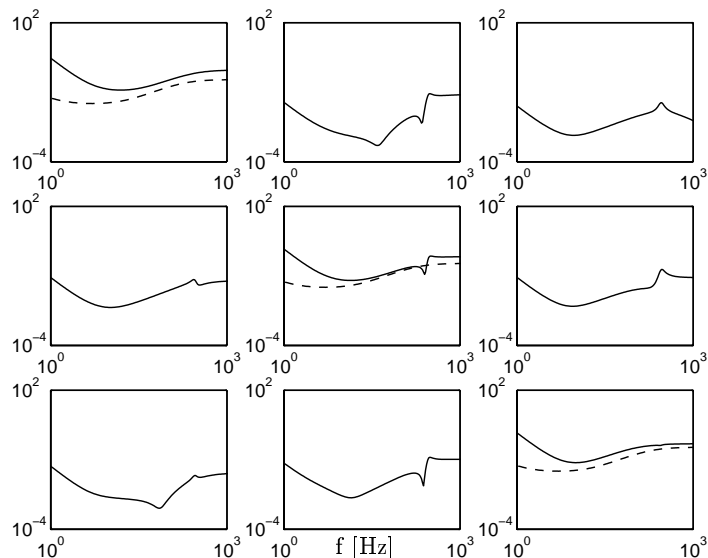


**Fig. 13.** Amplitude Bode plot of conventional parallel PID controller  $K_i$  (---) and newly designed 32nd-order multivariable controller  $K_{i+1}$  (—)

Before implementing the new controller the robust performance and stability needs to be evaluated. This can be done with the estimated set of models  $\mathcal{G}_i$  by evaluating  $\|J(G, K_{i+1})\|_\infty$  for all models  $G \in \mathcal{G}_i$ . Both stability and performance robustness of  $K_{i+1}$  can be evaluated with the structured singular value  $\mu\{M\}$  as indicated in (16). In Figure 14 the structured singular value is plotted point wise over the frequency range between 10 Hz and 1000 Hz for both the initial  $K_i$  and the newly designed feedback controller  $K_{i+1}$ . It can be observed that the newly designed controller  $K_{i+1}$  has improved the performance robustly, as the maximum of the structured singular value  $\mu\{M(e^{i\omega})\}$  has been lowered with a factor of approximately 4.

As a result, the performance index  $\|J(G, K_{i+1})\|_\infty$  evaluated for all models  $G \in \mathcal{G}_i$  with the new controller  $K_{i+1}$  is guaranteed to be four times better and as a result the performance of the closed-loop system has been improved robustly.

For presentation purposes, the weighting functions  $\hat{V}_i$  and  $\hat{W}_i$  that complete the set of models  $\mathcal{G}_i$  in (11) are scaled to normalize the uncertainty  $\Delta$ . As a result, *performance robustness* of the closed-loop system is guaranteed if  $\max_\omega \mu\{M(e^{i\omega})\} < 1$ . It can be seen from Figure 14 that this is not that case, but by adjusting the performance weighting functions  $U_1$  and  $U_2$  used in the performance characterization (8), performance robustness can be guaranteed for a specific choice of the weighting functions  $U_1$  and  $U_2$  in the performance criterion  $\|U_2 T(P, C) U_1\|_\infty$ . Whether or not the performance

weighting functions  $U_1$  and  $U_2$  are adjusted to guarantee performance robustness, the performance of the newly designed controller  $K_{i+1}$  has shown to be improved over the initial controller  $K_i$ .

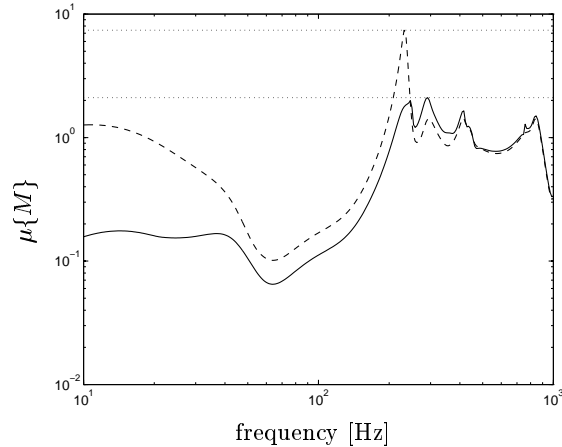


**Fig. 14.** Structured singular value  $\mu\{M(e^{i\omega})\}$  for initial controller  $K_i$  (dashed) and newly designed controller  $K_{i+1}$  (solid)

The newly designed controller  $K_{i+1}$  has been implemented on the positioning mechanism of the wafer stage and the performance robustness improvement can be clearly seen from the time domain plots. In order to illustrate the improved performance of the positioning control, the reference signals  $r_1$  and  $r_2$  depicted in Figure 5 are put on the newly designed feedback connection  $\mathcal{T}(G_0, K_{i+1})$ . A comparison with the servo error of Figure 6 obtained with the initial controller  $K_i$  is depicted in Figure 15. It can be seen from Figure 15 that both the speed and the accuracy of servo positioning have been improved successfully.

## 7 Summary

A wafer stage is part of a wafer stepper and used in chip manufacturing processes for accurate positioning of the silicon wafer on which the chips are to be produced. The wafer stage discussed in this application is a 3 degree of freedom (3DOF) positioning mechanism and the accurate positioning requirements of the wafer stage demand a robust and high-performance multivariable servo controller that enables a fast and accurate positioning of the wafer stage in 3DOF for a high throughput of silicon wafers.

This chapter illustrates the approximate and feedback relevant parametric identification of a wafer stage and shows how models along with an uncertainty characterization can be used to characterize a set of models. The set of

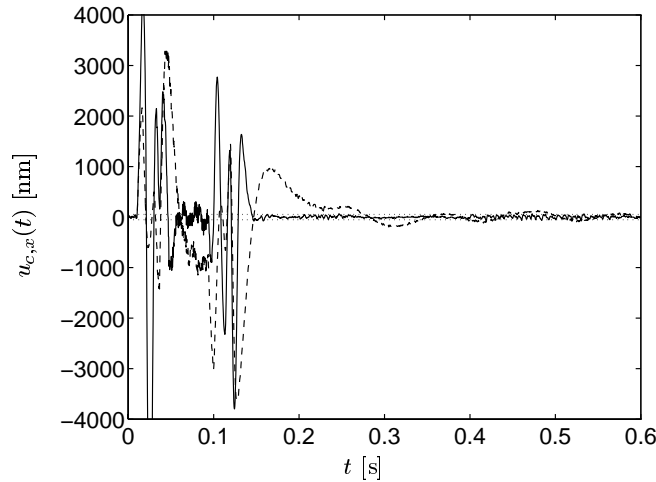


**Fig. 15.** Servo error response to a step in x-direction with initial parallel PID controller  $K_i$  (---) and newly designed multivariable controller  $K_{i+1}$  (—)

models is constructed within a framework of algebraic model representations that allows the incorporation of the controller information into the construction of the model set. It is shown that the set of models is particularly useful for the closed-loop and control relevant estimation of both the nominal model and the accompanying modeling error.

With the control relevant estimation of a model set and the use of robust control synthesis tools, both stability and performance robustness of the model-based robust control design can be monitored. Additionally, monitoring of the performance robustness enables the possibility to guarantee performance improvement in an iterative scheme of a control relevant estimation of a set of models followed by a robust control design. The procedure is shown to be suitable for the model-based robust control design of the wafer stage and is illustrated by a successful design and implementation of a robust controller.

## 8 Acknowledgements

The authors would like to acknowledge the support of Philips Research Laboratories, Eindhoven, the Netherlands for providing the wafer stepper experimental setup. Thanks also go to Okko Bosgra and Dick de Roover for fruitful discussions and their contributions to this paper.

## References

1. D.S. Bayard and R.Y. Chiang. A frequency domain approach to identification, uncertainty characterization and robust control design. In *Proc. 32nd IEEE Conference on Decision and Control*, pages 2266–2271, San Antonio, USA, 1993.
2. D.S. Bayard, Y. Yam, and E. Mettler. A criterion for joint optimization of identification and robust control. *IEEE Trans. on Automatic Control*, 37:986–991, 1992.
3. X. Bombois, M. Gevers, and G. Scorletti. A measure of robust stability for an identified set of parametrized transfer functions. *IEEE Trans. on Automatic Control*, 45:2141–2145, 2000.
4. P.M.M. Bongers. *Modeling and Identification of Flexible Wind Turbines and a Factorizational Approach to Robust Control*. PhD thesis, Delft University of Technology, Delft, the Netherlands, 1994.
5. R.A. de Callafon, D. Roover, and P.M.J. Van den Hof. Multivariable least squares frequency domain identification using polynomial matrix fraction descriptions. In *Proc. 35th IEEE Conference on Decision and Control*, pages 2030–2035, Kobe, Japan, 1996.
6. R.A. de Callafon and P.M.J. Van den Hof. Control relevant identification for  $H_\infty$ -norm based performance specifications. In *Proc. 34th IEEE Conference on Decision and Control*, pages 3498–3503, New Orleans, USA, 1995.
7. R.A. de Callafon and P.M.J. Van den Hof. Filtering and parametrization issues in feedback relevant identification based on fractional model representations. In *Proc. 3rd European Control Conference*, volume 1, pages 441–446, Rome, Italy, 1995.
8. R.A. de Callafon and P.M.J. Van den Hof. Suboptimal feedback control by a scheme of iterative identification and control design. *Mathem. Modelling of Systems*, 3(1):77–101, 1997.
9. R.G. Hakvoort. *System Identification for Robust Process Control: Nominal Models and Error Bounds*. PhD thesis, Delft University of Technology, Delft, the Netherlands, 1994.
10. R.G. Hakvoort and P.M.J. Van den Hof. Identification of probabilistic uncertainty regions by explicit evaluation of bias and variance errors. *IEEE Trans. Autom. Control*, 42(11), 1997.
11. R.G. Hakvoort, R.J.P. Schrama, and P.M.J. Van den Hof. Approximate identification with closed-loop performance criterion and application to LQG feedback design. *Automatica*, 30:679–690, 1994.
12. W.S. Lee, B.D.O. Anderson, R.L. Kosut, and I.M.Y. Mareels. A new approach to adaptive robust control. *Int. Journal of Adaptive Control and Signal Processing*, 7(3):183–211, 1993.
13. D. McFarlane and K. Glover. A loop shaping design procedure using  $H_\infty$  synthesis. *IEEE Trans. on Automatic Control*, 37:759–769, 1992.
14. B.M. Ninness and G.C. Goodwin. Estimation of model quality. *Automatica*, 31(12):1771–1797, December 1995.
15. R. Pintelon, P. Guillaume, Y. Rolain, J. Schoukens, and H. Van hamme. Parametric identification of transfer functions in the frequency domain - a survey. *IEEE Trans. on Automatic Control*, 39:2245–2260, 1994.

16. R.J.P. Schrama and O.H. Bosgra. Adaptive performance enhancement by iterative identification and control design. *Int. Journal of Adaptive Control and Signal Processing*, 7(5):475–487, 1993.
17. R.S. Smith and J.C. Doyle. Model validation: a connection between robust control and identification. *IEEE Trans. Autom. Control*, 37:942–952, 1992.
18. P.M.J. Van den Hof and R.J.P. Schrama. Identification and control - closed loop issues. *Automatica*, 31:1751–1770, 1995.
19. P.M.J. Van den Hof, R.J.P. Schrama, and P.M.M. Bongers. On nominal models, model uncertainty and iterative methods in identification and control design. *Lecture Notes in Control and Information Sciences*, 192:39–50, 1994.
20. P.M.J. Van den Hof, R.J.P. Schrama, R.A. de Callafon, and O.H. Bosgra. Identification of normalised coprime plant factors from closed-loop experimental data. *European Journal of Control*, 1(1):62–74, 1995.
21. M. Vidyasagar. *Control System Synthesis: A Factorization Approach*. MIT Press, Cambridge, Massachusetts, USA, 1985.
22. P.M.R. Wortelboer. *Frequency Weighted Balanced Reduction of Closed-Loop Mechanical Servo-Systems: Theory and Tools*. PhD thesis, Delft University of Technology, Delft, the Netherlands, 1993.
23. Z. Zang, R.R. Bitmead, and M. Gevers. Iterative weighted least-squares identification and weighted LQG control design. *Automatica*, 31:1577–1594, 1995.
24. K. Zhou, J.C. Doyle, and K. Glover. *Robust and Optimal Control*. Prentice-Hall, Upper Saddle River, New Jersey, USA, 1996.



# Index

- $\mu$ -synthesis, 17
- control
  - robust, 17
- control objective function, 11
- control-relevant identification, 19
- controller validation, 11
- coprime factor identification, 18
- dual-Youla uncertainty structure, 13
- iterative procedure, 10
- LFT, 14
- model set estimation, 10
- model uncertainty bounding, 16, 22, 23
- motion control, 1
- performance
  - assessment, 15
  - robustness, 11
- performance assessment, 10
- robust
  - control, 17
  - performance, 11, 15
- servo control design, 1
- uncertainty identification, 16
- wafer stepper, 1